**Proceedings of the ASME 2012 International Design Engineering Technical Conferences &
Computers and Information in Engineering Conference
IDETC/CIE 2012
August 12-15, 2012, Chicago, IL, USA**

DETC2012-70038

NONLINEAR ANALYSIS OF A 2-DOF PIECEWISE LINEAR AEROELASTIC SYSTEM

Tarek A. Elgohary
Department of Aerospace Engineering
Texas A&M University
College Station, Texas, 77843
Email: t.gohary@gmail.com

Tamás Kalmár-Nagy
Visiting Scholar
University of Illinois at Urbana-Champaign
Urbana - IL
Email: kalmarnagy@gmail.com

ABSTRACT

Aerodynamic forces for a 2-DOF aeroelastic system oscillating in pitch and plunge are modeled as a piecewise linear function. Equilibria of the piecewise linear model are obtained and their stability/bifurcations analyzed. Two of the main bifurcations are border collision and rapid/Hopf bifurcations. Continuation is used to generate the bifurcation diagrams of the system. Chaotic behavior following the intermittent route is also observed. To better understand the grazing phenomenon sets of initial conditions associated with the system behavior are defined and analyzed.

NOMENCLATURE

α Pitch DOF
y Plunge DOF
α_{eff} Effective angle of attack
α_{stall} Stall angle of attack
α_{switch} Angle of switch
α_{bound} Angle of model bound
$c_0 - c_4$ Line segments parameters
b Semichord of wing
S Wing span
m Mass of the system
k_y Spring constant plinge DOF
k_α Spring constant pitch DOF
c_y Viscous damping plunge DOF
c_α Viscous damping pitch DOF
I_{cg} Mass moment of inertia
ρ Air density
L Aerodynamic lift
M Aerodynamic moment
U Freestream velocity

INTRODUCTION

Nonlinear analysis of airfoils is a topic that is extensively covered in the literature [1–4]. In general, nonlinearities of airfoils are structural and/or aerodynamic. A comprehensive analysis for such nonlinearities was presented in [4]. The equations of motion of a 2D airfoil oscillating in pitch and plunge were derived. Cubic, freeplay and hysteresis nonlinearities were investigated. Numerical simulations investigating system stability, bifurcations and chaos were presented. Nonlinear aeroelasticity and its effects on flight and its association with limit cycle oscillations (LCO's) was investigated in [1]. Gilliat et al. [2] investigated both structural and aerodynamic nonlinearities with arising from stall conditions.

An experimental investigation of structural nonlinearity with emphasis given to continuous nonlinearities arising from spring hardening/softening effects was presented in [5], [6]. The aeroelastic response of a 2D airfoil with bilinear and cubic structural nonlinearities was investigated in [7]. Numerical simulations applying the finite difference method were compared against the analytical describing function method. LCO's were found to exist at a velocity below the divergent flutter limit. Chaotic behavior was investigated with the application of preload and bifurcation diagrams showing period doubling were plotted as a

1

Copyright © 2012 by ASME

result. Similarly, freeplay, hysteresis and cubic structural nonlinearities were analyzed in [8]. The flutter behavior of the airfoil was found to be highly dependent on initial conditions. LCO's existence arising from those nonlinearities was also investigated.

Aerodynamics nonlinearities were investigated separately in [9]. A typical airfoil section with transonic aerodynamic nonlinearities was analyzed using the describing function method. Results compared to numerical methods were found to be very close especially for small amplitudes of motion where the describing function method is very effective. Internal resonances in a 2D airfoil model with aerodynamic nonlinearities arising from dynamic stall was examined in [3]. The existence of internal resonances in specific classes of aeroelastic systems was investigated which lead to instabilities that were not predicted by traditional methods.

Combining both structural and aerodynamic nonlinearities was investigated in the aeroelastic response of a non rotating helicopter blade in [10] and [11]. The airfoil model was a NACA 0012 with three cases of nonlinearities, nonlinear structure linear aerodynamics, linear structure nonlinear aerodynamics and nonlinear structure with nonlinear aerodynamics, analyzed numerically. Structural nonlinearities were modeled by stiffness of freeplay whereas experimental data and curve fitting techniques were used to model the nonlinear aerodynamic lift coefficient. The flutter behavior in all cases was investigated and the amplitudes of LCO's were found to be dependent on freestream velocity and initial conditions. Chaotic behavior was also investigated for forced and unforced cases with Poincaré maps for certain velocities. Experimental and analytical results were found to be in good agreement. Freeplay, cubic and hysteresis structural nonlinearities were also investigated on 2 DOF and 3 DOF models. The analysis confirmed that the flutter amplitudes were largely dependent on initial conditions.

Representing a nonlinear continuous system as piecewise linear is generally used to approach the problem locally as independent linear systems which in many cases simplifies the problem and makes the solution more tractable. This approach was used in [12] with several problems involving forced and free oscillations. Hysteretic systems are also analyzed using this method, [13], where a hysteretic relay oscillator was analyzed, explicit solution of the problem was found and Poincaré maps of the system were constructed. In [14] and [15] the same approach was used to describe the behavior of an elasto-plastic beam model. The authors showed the hysteretic behavior of the system after finding the closed form solution of the problem and constructing a map for the determination of the plastic cycles of the system. The problem was tackled with both free and periodic impulse forcing oscillations. A piecewise linear oscillation model was utilized in [16] to analyze a single degree of freedom nonlinear oscillator with nonlinearity in the restoring force. The force was modeled as a piecewise linear function with a single change of slope. Poincaré maps of the system was also analyzed and harmonic, sub harmonic and chaotic motions were found with the bifurcations leading to them. Similarly, in [17] and [18], two types of piecewise linear systems were introduced and analyzed; systems with set up springs and systems with clearances. Sub harmonic and chaotic motions of those systems were also investigated and analyzed. Non smooth continuous systems equilibrium points bifurcations were examined in [19]. The so called 'multiple crossing bifurcations' where the Eigenvalues jump more than once over the imaginary axis were discussed for those types of systems with several examples of systems with that type of bifurcation.

THE AEROELASTIC SYSTEM
Aerodynamic Forces

A comprehensive experimental study was presented in [20] where lift coefficient vs. angle of attack data was collected for seven airfoil sections. All seven sections data had a piecewise linear nature similar to the NACA 0012 data shown in Fig. 1.

Motivated by the piecewise linear appearance of the data the lift coefficient, C_l, is modeled as a piecewise linear function of the effective angle of attack α_{eff}, Eqn. (1), which takes into account the instantaneous motion of the system.

$$\alpha_{eff} = \alpha + \frac{\dot{y}}{U}. \tag{1}$$

The piecewise linear model consists of three portions with boundaries defined by three values of α_{eff} designated as α_{stall}, α_{switch} and α_{bound}, as shown in Fig. 1. The first value describes the stall condition, α_{stall}, at which lift starts to decrease as α_{eff} is increased. The second value is a switching point at which the slope of C_l starts to increase again, α_{switch}. The third and final value defines the boundary of the model and consequently its validity over the presented range of angles of attack, α_{bound}. To sum up $C_l(\alpha_{eff})$ can be defined as

$$C_l(\alpha_{eff}) = \begin{cases} c_0 \alpha_{eff} \\ \quad \text{for } -\alpha_{stall} \leq \alpha_{eff} \leq \alpha_{stall} \\ c_1 \alpha_{eff} + \text{sgn}(\alpha_{eff}) c_2 \\ \quad \text{for } \alpha_{stall} \leq |\alpha_{eff}| \leq \alpha_{switch} \\ c_3 \alpha_{eff} + \text{sgn}(\alpha_{eff}) c_4 \\ \quad \text{for } \alpha_{switch} \leq |\alpha_{eff}| \leq \alpha_{bound}, \end{cases} \tag{2}$$

where, $c_0, c_1, \ldots, c_4$ are parameters characterized by the slopes describing the line segments of the lift function. Table 1 shows the values of these parameters and the values of the angles defining the boundary of each line segment.
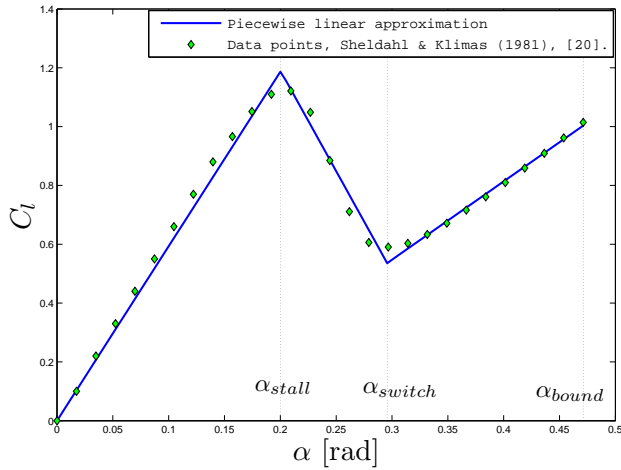
Copyright © 2012 by ASME

FIGURE 1. PIECEWISE LINEAR AERODYNAMIC MODEL

TABLE 1. LINE SEGMENTS PARAMETERS

Paramter	Value
c_0	5.932
c_1	-6.846
c_2	2.56
c_3	2.662
c_4	-0.2515
α_{stall}	0.2 rad
α_{switch}	0.2957 rad
α_{bound}	0.4712 rad

Dynamic model

The dynamic model is a typical 2 DOF, pitch and plunge, aeroelastic system with the assumption that the aeroelastic axis and the center of mass are collocated at three quarters of the chord length, Fig. 2.

The system equations are given by

$$m\ddot{y} + c_y\dot{y} + k_y y = -L(C_l(\alpha_{eff})), \qquad (3)$$

$$I_{cg}\ddot{\alpha} + c_\alpha\dot{\alpha} + k_\alpha\alpha = M(C_l(\alpha_{eff})). \qquad (4)$$
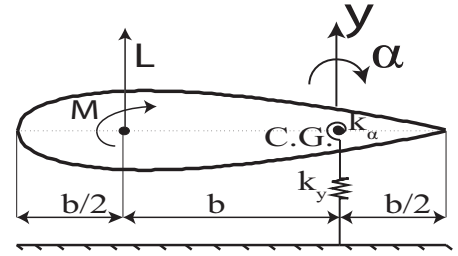
FIGURE 2. AEROELASTIC SYSTEM

The aerodynamic lift and moment as functions of the lift coefficient are given by

$$L(C_l(\alpha_{eff}))) = \rho U^2 b S C_l(\alpha_{eff}), \qquad (5)$$

$$M(C_l(\alpha_{eff})) = \rho U^2 b^2 S C_l(\alpha_{eff}). \qquad (6)$$

Table 2 shows the definition of all the system parameters shown in Fig. 2 and Eqn. (3) through (6).

Equations (1) to (6) are nondimensionalized by a length scale, L, a time scale, T, and a nondimensional freestream velocity, μ, given by

$$L^2 = \frac{I_{cg}}{\rho b^2 S}, \quad T^2 = \frac{m}{k_y}, \quad \mu = \frac{U}{L/T}. \qquad (7)$$

These scales yield a nondimensional plunge, $\tilde{y} = \frac{y}{L}$, a nondimensional time, $\tau = \frac{t}{T}$, and the derivative w.r.t nondimensional time (τ), $()' = \frac{d()}{d\tau}$. Carrying out the nondimensionalization of Eqn. (1) to (6), and substituting with Eqn. (7) the system equations can be expressed as

$$\alpha_{eff} = \alpha + \frac{1}{\mu}\tilde{y}'. \qquad (8)$$

For $-\alpha_{stall} \leq \alpha_{eff} \leq \alpha_{stall}$

$$\tilde{y}'' + (p_1 + p_2\mu c_0)\tilde{y}' + \tilde{y} + p_2\mu^2 c_0\alpha = 0, \qquad (9)$$
$$\alpha'' + p_3\alpha' + (p_4 - \mu^2 c_0)\alpha - \mu c_0\tilde{y}' = 0,$$

3

Copyright © 2012 by ASME

Paramter	Description	Value/Units
b	Semichord of wing	0.1064 m
S	Wing span	0.6 m
m	System mass	12 Kg
k_y	Spring constant plunge DOF	2844.4 N/m
k_α	Spring constant pitch DOF	2.82 N.m/rad
c_y	Viscous damping plunge DOF	27.43 Kg/s
c_α	Viscous damping pitch DOF	0.036 Kg.m^2/s
I_{cg}	Mass moment of inertia	0.0433 Kg.m^2
ρ	Air density	1.2 Kg/m^3
L	Aerodynamic lift	N
M	Aerodynamic moment	N.m
y	Plunge DOF	m
α	Pitch DOF	rad
U	Freestream velocity	m/s

For $\alpha_{stall} \leq |\alpha_{eff}| \leq \alpha_{switch}$

$$\tilde{y}'' + (p_1 + p_2\mu c_1)\tilde{y}' + \tilde{y} + p_2\mu^2 c_1\alpha + \mathrm{sgn}(\alpha_{eff})\mu^2 c_2 = 0,$$
$$\alpha'' + p_3\alpha' + (p_4 - \mu^2 c_1)\alpha - \mu c_1\tilde{y}' + \mathrm{sgn}(\alpha_{eff})\mu^2 c_2 = 0. \tag{10}$$

For $\alpha_{switch} \leq |\alpha_{eff}| \leq \alpha_{bound}$

$$\tilde{y}'' + (p_1 + p_2\mu c_3)\tilde{y}' + \tilde{y} + p_2\mu^2 c_3\alpha + \mathrm{sgn}(\alpha_{eff})\mu^2 c_4 = 0,$$
$$\alpha'' + p_3\alpha' + (p_4 - \mu^2 c_3)\alpha - \mu c_3\tilde{y}' + \mathrm{sgn}(\alpha_{eff})\mu^2 c_4 = 0. \tag{11}$$

The nondimensional parameters p_1, p_2, p_4 and p_4 are given by

$$p_1 = \frac{c_y}{\sqrt{mk_y}}, \qquad p_2 = \frac{\sqrt{\rho I_{cg}S}}{m},$$
$$p_3 = \frac{c_\alpha}{I_{cg}}\sqrt{\frac{m}{k_y}}, \qquad p_4 = \frac{k_\alpha m}{I_{cg}k_y}. \tag{12}$$

THE BILINEAR MODEL

The governing equations of the bilinear model are extracted from Eqn. (9) and (10) as

For $-\alpha_{stall} \leq \alpha_{eff} \leq \alpha_{stall}$
$$\tilde{y}'' + (p_1 + p_2\mu c_0)\tilde{y}' + \tilde{y} + p_2\mu^2 c_0\alpha = 0, \tag{13}$$
$$\alpha'' + p_3\alpha' + (p_4 - \mu^2 c_0)\alpha - \mu c_0\tilde{y}' = 0.$$

For $\alpha_{stall} < |\alpha_{eff}|$
$$\tilde{y}'' + (p_1 + p_2\mu c_1)\tilde{y}' + \tilde{y} + p_2\mu^2 c_1\alpha + \mathrm{sgn}(\alpha_{eff})\mu^2 c_2 = 0,$$
$$\alpha'' + p_3\alpha' + (p_4 - \mu^2 c_1)\alpha - \mu c_1\tilde{y}' + \mathrm{sgn}(\alpha_{eff})\mu^2 c_2 = 0. \tag{14}$$

Equation (14) is assumed to be unbouded with $\alpha_{switch} \to \infty$. This assumption lets the bilinear model exceed the physical bounds of the original aeroelastic system resulting in a more general solution that can be applied to several classes of problems, [21], [22]. Figure 3 shows the full bilinear model and the odd nature of the lift coefficient funciton.
Using the state trnasformation

$$x_1 = \tilde{y}, \quad x_2 = \tilde{y}', \quad x_3 = \alpha, \quad x_4 = \alpha'. \tag{15}$$

Equations (8), (13) and (14) are put in state space form as

For $-\alpha_{stall} \leq \alpha_{eff} \leq \alpha_{stall}$ [System I]
$$\begin{bmatrix} \dot{x_1} \\ \dot{x_2} \\ \dot{x_3} \\ \dot{x_4} \end{bmatrix} = \begin{bmatrix} 0 & 1 & 0 & 0 \\ -1 & -(p_1+p_2\mu c_0) & -p_2\mu^2 c_0 & 0 \\ 0 & 0 & 0 & 1 \\ 0 & \mu c_0 & -(p_4-\mu^2 c_0) & -p_3 \end{bmatrix} \begin{bmatrix} x_1 \\ x_2 \\ x_3 \\ x_4 \end{bmatrix}. \tag{16}$$

For $\alpha_{stall} < |\alpha_{eff}|$ [System II]
$$\begin{bmatrix} \dot{x_1} \\ \dot{x_2} \\ \dot{x_3} \\ \dot{x_4} \end{bmatrix} = \begin{bmatrix} 0 & 1 & 0 & 0 \\ -1 & -(p_1+p_2\mu c_1) & -p_2\mu^2 c_1 & 0 \\ 0 & 0 & 0 & 1 \\ 0 & \mu c_1 & -(p_4-\mu^2 c_1) & -p_3 \end{bmatrix} \begin{bmatrix} x_1 \\ x_2 \\ x_3 \\ x_4 \end{bmatrix}$$
$$+ \begin{bmatrix} 0 \\ -p_2\mu^2 c_2 \\ 0 \\ \mu^2 c_2 \end{bmatrix} \mathrm{sgn}(\alpha_{eff}). \tag{17}$$

where the two portions of the bilinear model are defined in Eqn. (16) and (17) as System I and System II, respectively. A similar
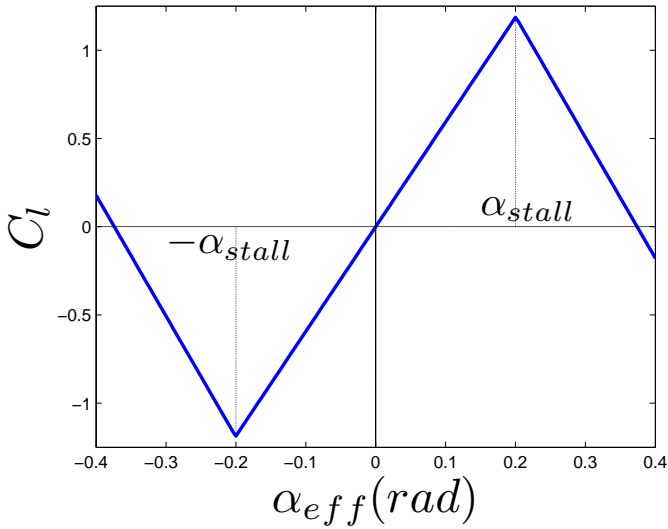
4

FIGURE 3.   BILINEAR AERODYNAMIC MODEL

state transformation expression can also be shown for α_{eff} as

$$\alpha_{eff} = x_3 + \frac{1}{\mu}x_2. \tag{18}$$

Equilibrium Points

Each of System I and System II equilibria are obtained to represent the overall bilinear system equilibrium points. System I can be represented in the general form $\underline{\dot{x}} = A_I \underline{x}$ hence its equilibrium is $\underline{x}_{Ieq} = \begin{bmatrix} 0 & 0 & 0 & 0 \end{bmatrix}^T$. For system II the general form is $\underline{\dot{x}} = A_{II}\underline{x} + \underline{b}$. The equilibrium vector can be obtained from solving $\underline{x}_{IIeq} = -A_{II}^{-1}\underline{b}$. Hence,

$$\underline{x}_{IIeq} = \pm \begin{bmatrix} -p_2\mu^2c_2 + \frac{p_2\mu^4c_1c_2}{-p_4+\mu c_1} \\ 0 \\ -\frac{\mu^2c_2}{-p_4+\mu^2c_1} \\ 0 \end{bmatrix} \tag{19}$$

In order for this equilibrium to exist it has to lie within System II domain. Hence, Eqn. (19) must satisfy the inequality condition of System II in Eqn. (17). Substituting Eqn. (19) into Eqn. (18) yields the value of μ at which system II equilibrium exists in its domain, μ_{IIeq},

$$\mu_{IIeq}^2 \geq \frac{\alpha_{stall}p_4}{c_2 + \alpha_{stall}c_1}. \tag{20}$$

Stability Analysis

The characteristic polynomials for systems I and II are expressed as

For system I

$$\begin{aligned} f_I(\lambda) = &\lambda^4 + (p_3 + p_1 + p_2\mu c_0)\lambda^3 \\ &+ (1 + p_4 - \mu^2c_o + p_3p_1 + p_3p_2\mu c_0)\lambda^2 \\ &+ (p_4p_1 + p_4p_2\mu c_0 - \mu^2c_op_1 + p_3)\lambda + p_4 - \mu^2c_o \end{aligned} \tag{21}$$

For system II

$$\begin{aligned} f_{II}(\lambda) = &\lambda^4 + (p_3 + p_1 + p_2\mu c_1)\lambda^3 \\ &+ (1 + p_4 - \mu^2c_1 + p_3p_1 + p_3p_2\mu c_1)\lambda^2 \\ &+ (p_4p_1 + p_4p_2\mu c_1 - \mu^2c_1p_1 + p_3)\lambda + p_4 - \mu^2c_1 \end{aligned} \tag{22}$$

Applying the Liénard-Chipart stability criterion [23] to Eqn. (21) and (22) the values of μ for which each system is found to lose stability is obtained.

$$\text{For system I,} \qquad \mu_I^2 = \frac{p_4}{c_0}. \tag{23}$$

For system II,

$$\begin{aligned} p_4 - \mu_{II}^2 = &\frac{p_4p_1 + p_3 - p_1c_1\mu_{II}^2 + p_4p_2c_1\mu_{II}}{p_3 + p_1 + p_2c_1\mu_{II}} \\ &(1 + p_4 + p_3p_1 - c_1\mu_{II}^2 + p_3p_2c_1\mu_{II} \\ &- \frac{p_4p_1 + p_3 - p_1c_1\mu_{II}^2 + p_4p_2c_1\mu_{II}}{p_3 + p_1 + p_2c_1\mu_{II}}). \end{aligned} \tag{24}$$

Figure 4(a) shows the eigenvalues behavior of System I as two of the complex conjugate imaginary eigenvalues move towards the origin. At $\mu = \mu_I$ they collide and become real with one on the right half plane causing System I equilibrium to lose stability. This is a case of colliding eigenvalues, [24], which at $\mu = \mu_I$ causes the trajectory to shift oscillatory to exponential as the solution converges towards $\underline{x}_{Ieq}$ as shown in Fig. 5. For System II, Fig. 4(b), a pair of complex conjugate eigenvalues cross to the right half plane rendering System II equilibrium unstable.

Bifurcations Of Equilibrium Points

The bilinear system undergoes a border collision bifurcation, [25], [26], as System I loses stability, $\mu = \mu_I$, exactly when System II equilibrium lies on the boundary or the border between

5

Copyright © 2012 by ASME
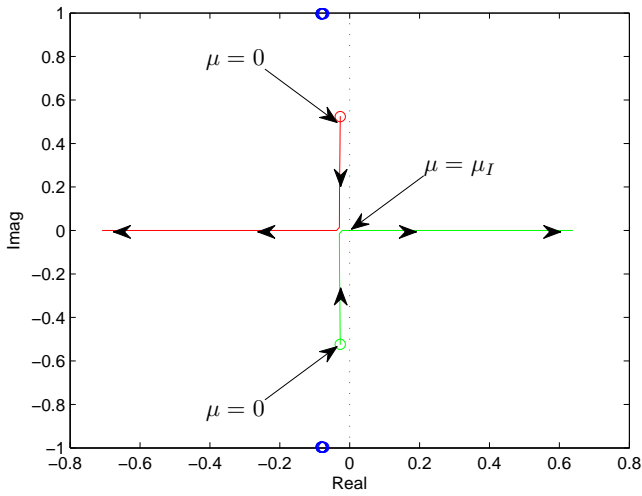
(a) SYSTEM I EIGENVALUES
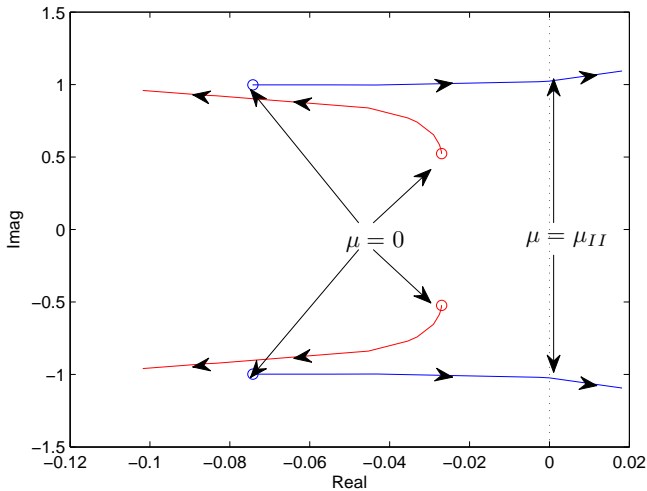
(b) SYSTEM II EIGENVALUES

FIGURE 4. BILINEAR MODEL EIGENVALUES BEHAVIOR

the two systems. Steps shown in Eqn. (25) show the derivation of that phenomenon.

$$\mu_I^2 = \frac{p_4}{c_0} = \frac{p_4 \alpha_{stall}}{c_0 \alpha_{stall}}$$

System II equilibrium exists on the border at,

$$\mu_{IIeq}^2 = \frac{p_4 \alpha_{stall}}{c_1 \alpha_{stall} + c_2} \tag{25}$$

At $\quad \left| \alpha_{eff} \right| = \alpha_{stall}, \quad c_0 \alpha_{stall} = c_1 \alpha_{stall} + c_2$

Hence,

$$\mu_I = \mu_{IIeq}$$
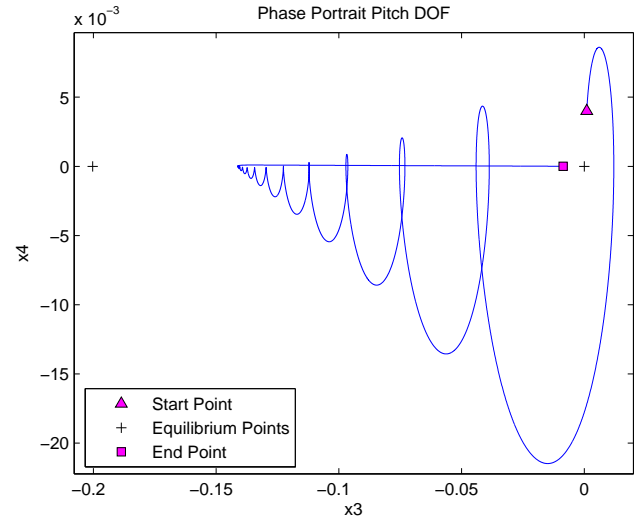
FIGURE 5. PITCH DOF PHASE PORTRAIT @ $\mu = \mu_I$

As the value of μ is increased two of the complex conjugate eigenvalues of System II move towards the imaginary axis crossing it at $\mu = \mu_{II}$, Fig. 4(b). System II stable node loses stability and a stable limit cycle is created as a result of a rapid bifurcation. Rapid bifurcations, [21] and [22], are analogous to Hopf bifurcations in continuous systems [27], they differ in the limit cycle amplitude propagation as it does not follow the square root scaling rule where the amplitude is not proportional to $O(\mu^{\frac{1}{2}})$.

The bifurcation diagrams for the pitch and plunge DOF are generated numerically utilizing MATCONT, [28], as shown in Fig. 6(a) and 6(b), respectively.

NUMERICAL RESULTS

Numerical simulations for the bilinear system dynamics are presented here. The phase portraits of the pitch DOF, (x_3, x_4) plane, along with a projection of the (x_3, x_2) plane are presented. This way both the system dynamics, represented in the pitch DOF phase portrait, and the switching phenomenon are presented and the relation between them clarified. Chaotic behavior of the system is also investigated and anlayzed numerically. The complete set of results is preseneted in [29].

Figure 7 shows the convergence towards System I stable equilibrium, $\underline{x}_{Ieq}$, for $\mu < \mu_I$. For $\mu_I < \mu < \mu_{II}$ trajectories converge to System II stable equilibrium, $\underline{x}_{IIeq}$, as shown in Fig. 8. The stable limit cycle arising from the rapid bifurcation for a value of $\mu > \mu_{II}$ is shown in Fig. 9. The chaotic behavior is investigated numerically and presented as a demonstation of the full nonlinear potential of piecewise linear systems. The chaotic behavior is observed in the bilinear model dynamics via the intermittent route to chaos, [30]. The bilinear model follows a type 1 intermittency
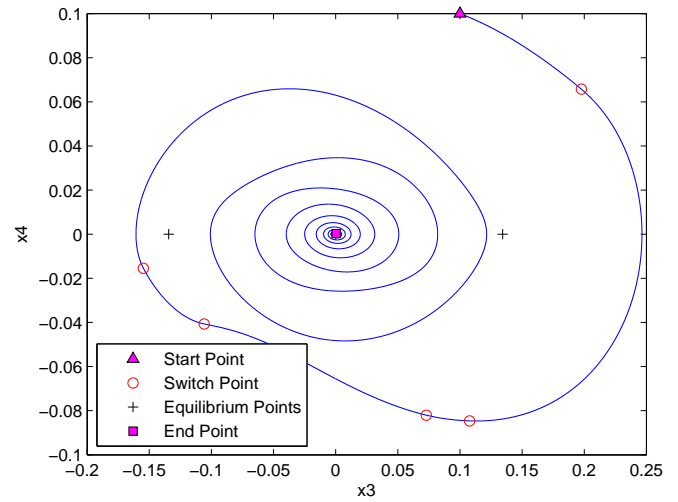
6

Copyright © 2012 by ASME
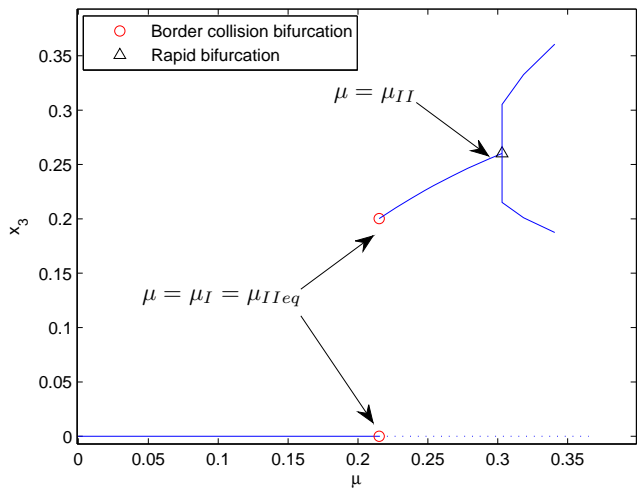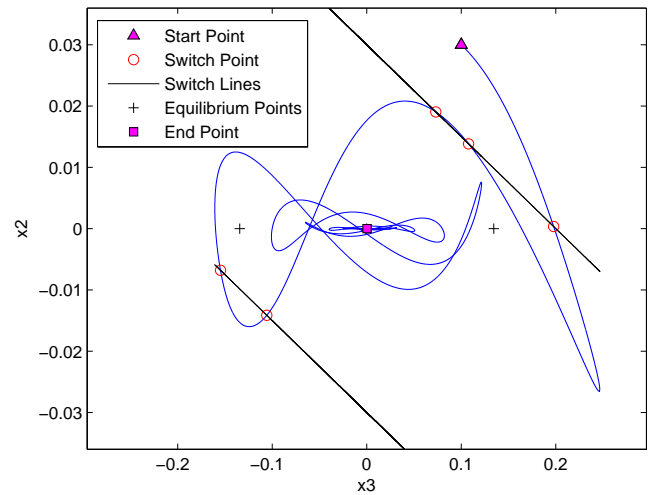
(a) PITCH DOF EQUILIBRIUM BIFURCATION DIAGRAM
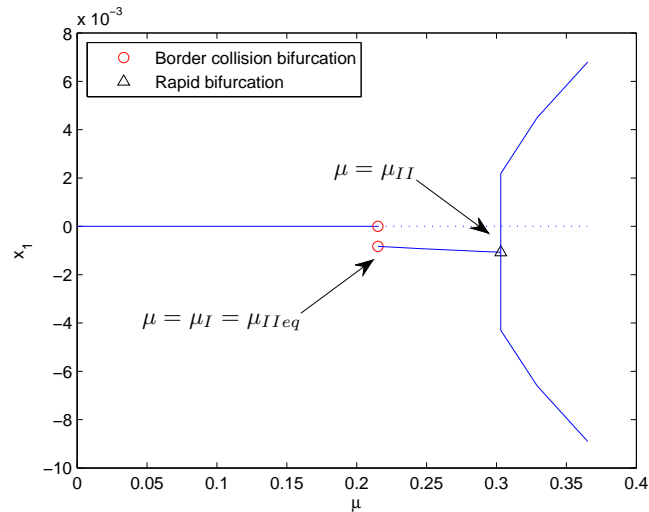
(b) PLUNGE DOF EQUILIBRIUM BIFURCATION DIAGRAM

FIGURE 6. EQUILIBRIA BIFURCATION DIAGRAMS

(a) (x_3, x_4) PLANE

(b) (x_3, x_2) PLANE

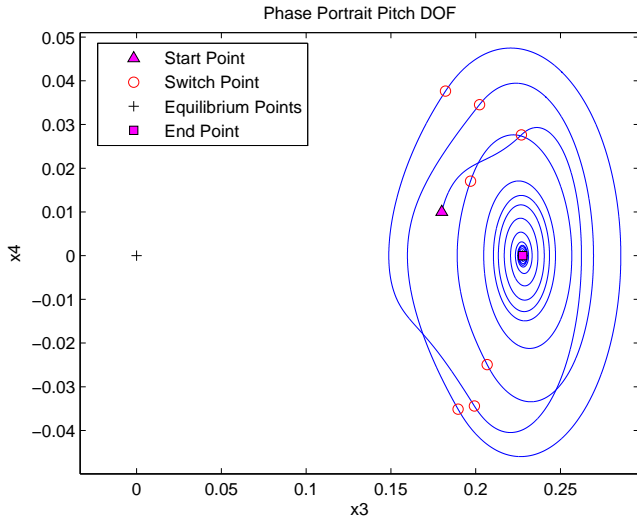**FIGURE 7**. SIMULATION FOR $\mu < \mu_I, \mu = 0.15$

as one of the Floquet multipliers crosses the unit circle along the real axis at +1. This type of intermittency leads to bursts of chaotic behavior with the existence of the stable periodic amplitudes hence the name stable intermittency. This type has been widely observed in many experiments in [31], [32] and [33]. The numerical results, Fig. 10, show the chaotic behavior of the system in the (x_3, x_2) plane as the values of μ is changed. The stable periodic amplitude can be observed around the switching lines along with the chaotic jumps back and forth between them. The coexistence of a pure periodic and a chaotic solution has been observed at the same value of $\mu = 0.7$ as shown in Fig. 11. In this case for the same value of μ and depending on the initial

conditions the system will converge to either a chaotic solution, Fig. 11(a), or a stable periodic solution, Fig. 11(b).
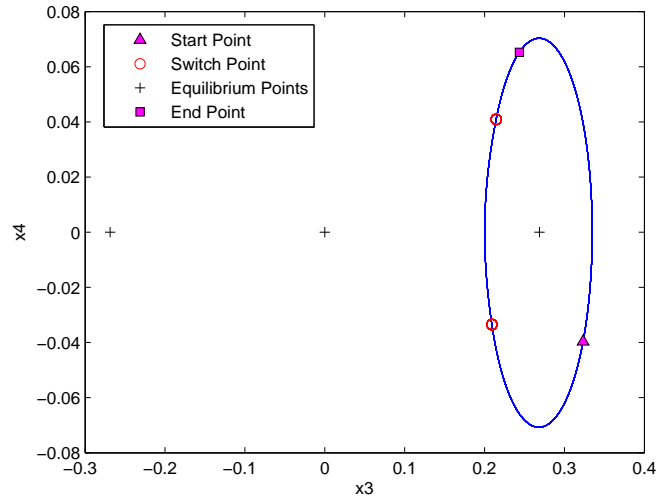
SETS OF INITIAL CONDITIONS

In this section sets of initial conditions lying on the switching line are defined and analyzed to better understand and verify the dynamical analysis of the bilinear system. The set of initial conditions lying on the switching line, L, can be defined as,
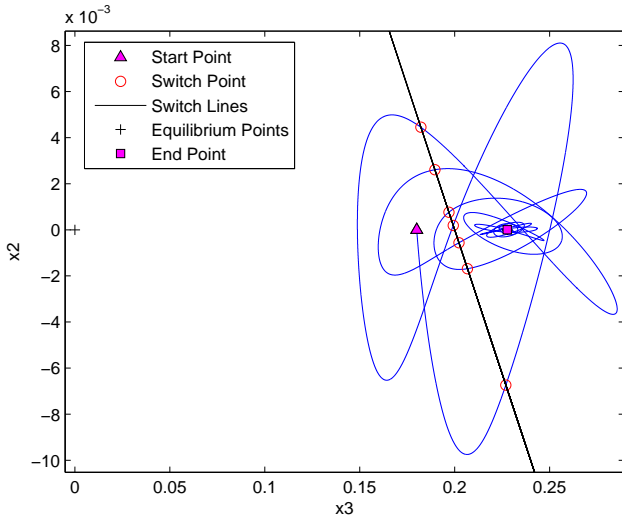
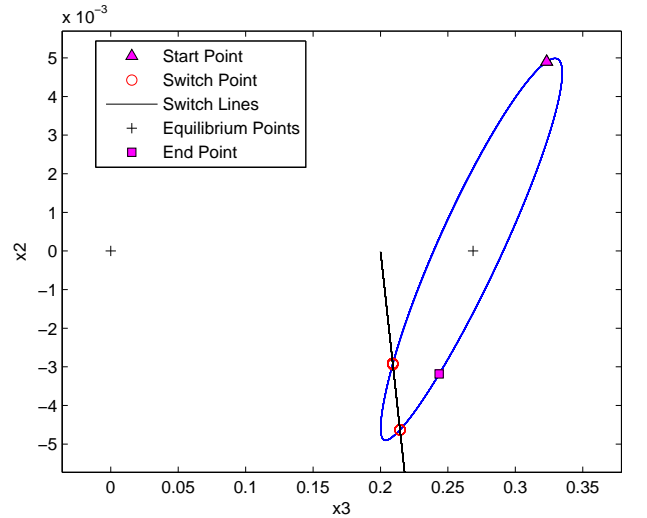$$L = \{\underline{x} | x_2 = \mu(\pm \alpha_{stall} - x_3)\}. \tag{26}$$

7 Copyright © 2012 by ASME

(a) (x_3, x_4) PLANE

(b) (x_3, x_2) PLANE

FIGURE 8. SIMULATION FOR $\mu_I < \mu < \mu_{II}, \mu = 0.25$

(a) (x_3, x_4) PLANE

(b) (x_3, x_2) PLANE

FIGURE 9. SIMULATION FOR $\mu > \mu_{II}, \mu = 0.32$

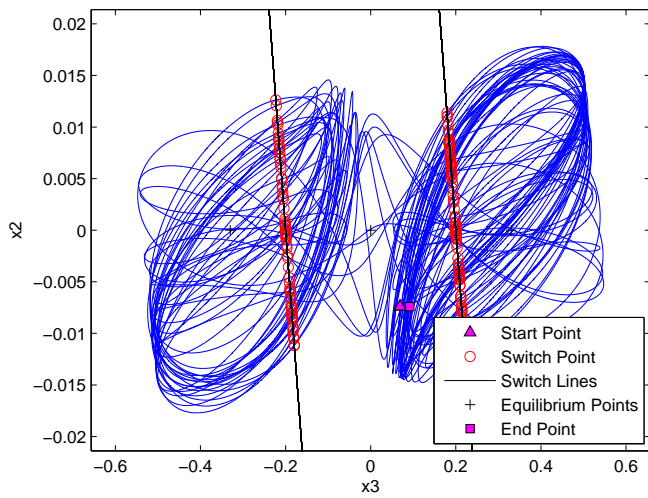The equation of the switch line can be written as,

$$w(x_3, x_2) = x_2 - f(x_3) \quad \text{where, } f(x_3) = \mu(\alpha_{stall} - x_3). \quad (27)$$

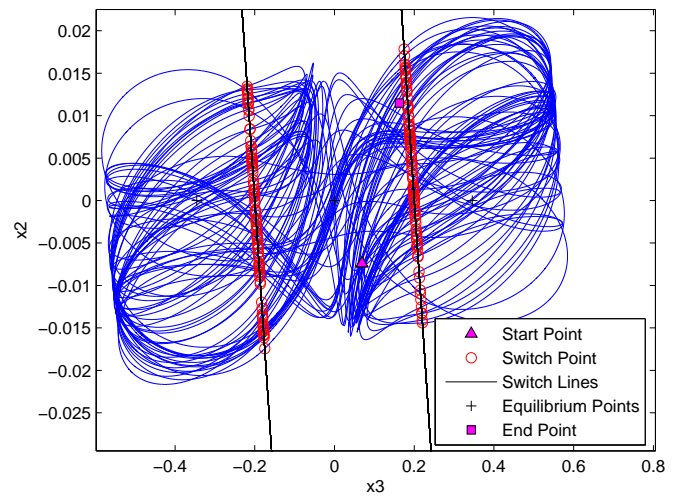Hence, the unit vector describing the equation of the switch line is expressed as

$$\hat{\underline{v}} = (v_1, v_2) = \left(\frac{1}{\sqrt{1+\mu^2}}, \frac{-\mu}{\sqrt{1+\mu^2}} \right) \quad (28)$$

Taking the directional derivative of $w(x_3, x_2)$ along $\hat{\underline{v}}$ and substituting with the dynamics, L can be divided into three main subsets based on the direction of the flow of a point in L. The first subset, Eqn. (29), describes a point starting in L and moving into System II crossing over from System I, Fig. 12(a). The second subset, Eqn. (30), defines a point in L going into System I crossing over from System II, Fig. 12(b). The third and final set, Eqn. (31), describes points in L that do not cross to either system but stay in the same domain. In other words S_G set describes the grazing case where a point touches the switching line and never
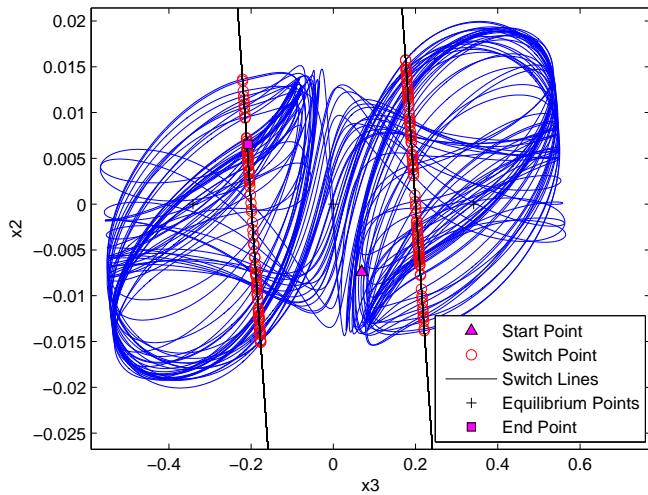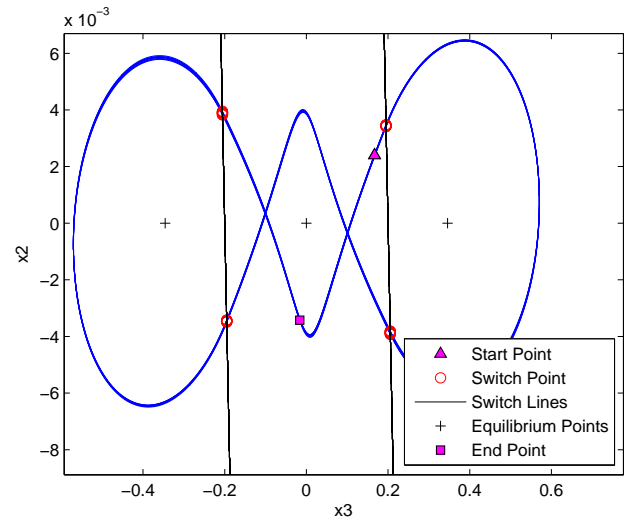
8

Copyright © 2012 by ASME

(a) (x_3, x_2) PLANE, $\mu = 0.55$

(b) (x_3, x_2) PLANE, $\mu = 0.65$

FIGURE 10. INTERMITTENT CHAOTIC BEHAVIOR

(a) CHAOTIC SOLUTION, $\mu = 0.7$

(b) PERIODIC SOLUTION, $\mu = 0.7$

FIGURE 11. CO-EXISTENCE OF CHAOTIC AND PERIODIC SOLUTIONS @ $\mu = 0.7$

crosses to the other side, Fig. 12(c).

$$S_{I-II} = \left\{ \underline{x} | \underline{x} \in L, |x_1 - \mu x_4| < -p_1 x_2 - p_2 \mu^2 c_o \alpha_{stall} \right\} \quad (29)$$

$$S_{II-I} = \left\{ \underline{x} | \underline{x} \in L, |x_1 - \mu x_4| > -p_1 x_2 - p_2 \mu^2 c_o \alpha_{stall} \right\} \quad (30)$$

$$S_G = \left\{ \underline{x} | \underline{x} \in L, |x_1 - \mu x_4| = -p_1 x_2 - p_2 \mu^2 c_o \alpha_{stall} \right\} \quad (31)$$

The subsets of L in Eqn. (29, 30,31) are further disected into smaller subsets. S_{I-II} has C_I, Eqn. (32a), the set of initial conditions in S_{I-II} that in a finite time T would come back and cross the switch line as elements of S_{II-I}. E_{II}, Eqn. (32b), the points in S_{I-II} that would as $t \to \infty$ converge to system II equilibrium. G_{II}, Eqn. (32c), the points that in a finite time T would come back to the switch line and graze it without crossing to System I hence belonging to S_G. Finally H, Eqn. (32d), the set of points
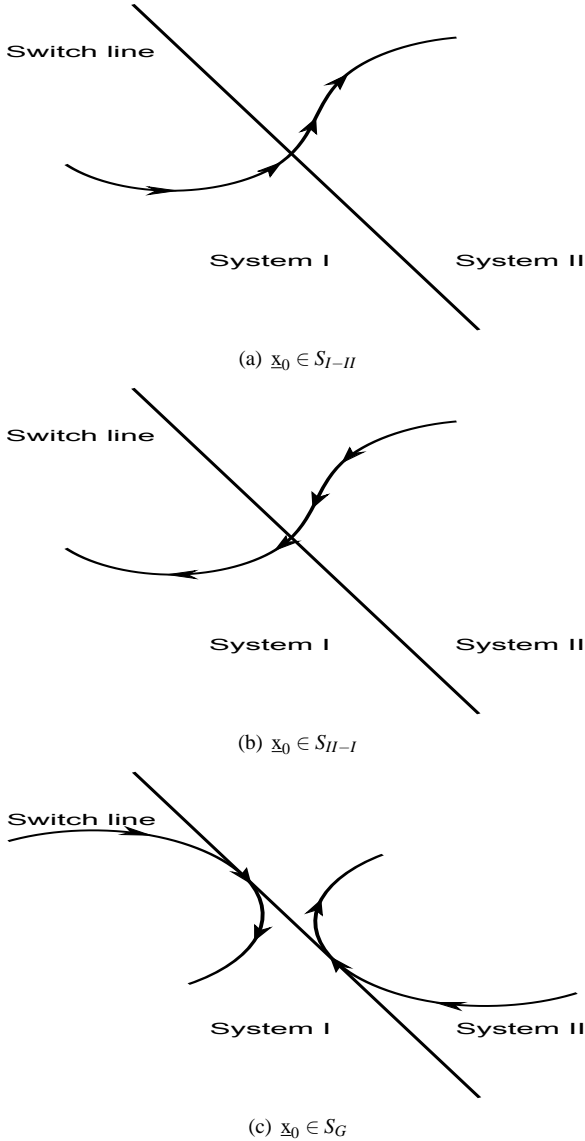
9 Copyright © 2012 by ASME

$$H = \left\{\vec{y} \,\middle|\, \vec{y} \in S_{I-II}, \lim_{t \to \infty} \|\vec{x}(t)\| = \infty, \right.$$
$$\left. \vec{x}(0) = \vec{y}, \vec{x}(t > 0) \notin L \right\} \tag{32d}$$

Similar to the subsets of S_{I-II}, S_{II-I} can be disected in the same manner. As shown in (33) there exists 3 main subsets to describe the evolution of points in S_{II-I}. C_{II}, Eqn. (33a), for points coming back to the switch line in finite time T and crossing it as elements of S_{I-II}. E_I, Eqn. (33b), for points converging to $\underline{x}_{Ieq}$ as $t \to \infty$. Finally, G_I, Eqn. (33c), for the grazing condition on System I side of the switching line.

$$C_I I = \left\{ \vec{y} \,\middle|\, \vec{y} \in S_{II-I}, \vec{x}(T) \in S_{I-II}, \vec{x}(0) = \vec{y} \right\} \tag{33a}$$

$$E_I = \left\{ \vec{y} \,\middle|\, \vec{y} \in S_{II-I}, \lim_{t \to \infty} \vec{x}(t) = \vec{x}_{Ieq}, \right.$$
$$\left. \vec{x}(0) = \vec{y}, \vec{x}(t > 0) \notin L \right\} \tag{33b}$$

$$G_I = \left\{ \vec{y} \,\middle|\, \vec{y} \in S_{II-I}, \vec{x}(T) \in S_G, \vec{x}(0) = \vec{y} \right\} \tag{33c}$$

It is clear that the definitions obtained for the various subsets of L agree with the results obtained from the stability analysis and the bifurcation of equilibrium points. Those definitions can be considered an alternative way to analyze systems with switching surfaces. Another use for such subsets is to develop Poincaré maps utilizing the relationships defined above and tracing the behavior of a point on the switching line subject to the system dynamics.

DISCUSSION AND CONCLUSION

Nonlinear analysis of aeroelastic systems is a topic that has been widely covered in the literature. The nonlinearities introduced to aeroelastic systems can be either aerodynamic nonlinearities, structural nonlinearities or a mixture of both. Many models were introduced to address these nonlinearities and study their effects on aeroelastic systems. In this research project aerodynamic nonlinearities arising from the stall behavior of an aeroelastic system were studied. A piecewise linear model utilizing experimental data for the lift coefficient versus the angle of attack for a NACA 0012 airfoil was proposed and analyzed.

The piecewise linear model was proposed to describe the lift coefficient as a function of the effective angle of attack. The equations of motion for the system were introduced and nondimensionalized. The nondimensionalizing introduced both time and length scales that were used to nondimensionalize the system states, pitch and plunge, along with the freestream velocity which defined the system bifurcation parameter.

(a) $\underline{x}_0 \in S_{I-II}$

(b) $\underline{x}_0 \in S_{II-I}$

(c) $\underline{x}_0 \in S_G$

FIGURE 12. SUBSETS OF L

that would go unbounded as $t \to \infty$.

$$C_I = \left\{ \vec{y} \,\middle|\, \vec{y} \in S_{I-II}, \vec{x}(T) \in S_{II-I}, \vec{x}(0) = \vec{y} \right\} \tag{32a}$$

$$E_{II} = \left\{ \vec{y} \,\middle|\, \vec{y} \in S_{I-II}, \lim_{t \to \infty} \vec{x}(t) = \vec{x}_{IIeq}, \right.$$
$$\left. \vec{x}(0) = \vec{y}, \vec{x}(t > 0) \notin L \right\} \tag{32b}$$

$$G_{II} = \left\{ \vec{y} \,\middle|\, \vec{y} \in S_{I-II}, \vec{x}(T) \in S_G, \vec{x}(0) = \vec{y} \right\} \tag{32c}$$

10 Copyright © 2012 by ASME

A simplified bilinear model was then extracted from the full piecewise linear model and analyzed. Equilibrium points of the bilinear model were found analytically and represented as a function of the bifurcation parameter. The stability of those equilibrium points was then checked applying the Liénard-Chipart theorem. From the stability checks the values of the non dimensional freestream velocity at which equilibrium points loses stability are calculated. Bifurcation diagrams of the system are then shown utilizing MATCONT. Two types of bifurcations are analyzed; the border collision bifurcation which described the existence of System II equilibrium and the loss of stability of System I and the rapid bifurcation which explains the onset of a stable limit cycle as system II loses stability. sets of initial conditions of the system are introduced to describe the various system behavior examined in the bifurcation diagrams and numerical simulation. Those sets describe initial conditions starting on the boundary between system I and II and how they get mapped with respect to each other. Numerical results were also presented to show those sets and the mapping between them. By defining and understanding the behavior of those sets the system local and global behavior is examined and analyzed. Finally, Chaotic behavior was also investigated and observed in the intermittent route to chaos. The system exhibited jumps from periodic to chaotic solutions. The route to chaos and the coexistence of both periodic and chaotic solutions were shown numerically. As a result of this study the local and global system behavior was analyzed and understood. Interesting phenomena was observed in this analysis such as the intermittent chaotic behavior and the jumps between the system boundaries associated with it. Also the analysis introduced new types of bifurcations that are internsic to piecewise systems such as border collision and the rapid bifurcations.

Finally, it is important to highlight that some of the results presented in this work exceed the boundaries of the physical validity of the model for an airfoil. The chaotic behavior observed can be attributed to the continuity of the model beyond the shown range. The analysis was conducted on the bilinear model assuming no restrictions on the range of the angle of attack. This enabled us to understand the full behavior of such models and their behavior.

ACKNOWLEDGMENT

REFERENCES

[1] Dowell, E., Edwards, J., and Strganac, T., 2003. "Nonlinear aeroelasticity". *Journal of Aircraft, 40*(5), p. 857.

[2] Gilliatt, H. C., Strganac, T. W., and Kurdila, A. J., 1997. "Nonlinear aeroelastic response of an airfoil". AIAA 97-459.

[3] Gilliatt, H. C., Strganac, T. W., and Kurdila, A. J., 2003. "An investigation of internal resonance in aeroelastic systems". *Nonlinear Dynamics, 31*, pp. 1–22.

[4] Lee, B. H. K., Price, S. J., and Wong, Y. S., 1999. "Nonlinear aeroelastic analysis of airfoils: bifurcation and chaos". *Progress in Aerospace Sciences, 35*(3), pp. 205 – 334.

[5] O'Neil, T., Gilliatt, H. C., and Strganac, T. W., 1996. "Investigations of aeroelastic response for a system with continuous structural nonlinearities". AIAA 96-1390.

[6] ONeil, T., and Strganac, T. W., 1998. "Aeroelastic response of a rigid wing supported by nonlinear springs". *Journal of Aircraft, 35*, pp. 616–622.

[7] Price, S. J., Alighanbari, H., and Lee, B. H. K., 1995. "The aeroelastic response of a 2-dimensional airfoil with bilinear and cubic structural nonlinearities". *Journal of Fluids and Structures, 9*, pp. 175–193.

[8] Woolston, D. S., Runyan, H. L., and Andrews, R. E., 1957. "An investigation of effects of certain types of structural nonlinearities on wing and control surface flutter". *Journal of the Aeronautical Sciences, 24*, pp. 57–63.

[9] Ueda, T., and Dowell, E. H., 1984. "Flutter analysis using nonlinear aerodynamic forces". *Journal of Aircraft, 21*, pp. 101–109.

[10] Tang, D. M., and Dowell, E. H., 1992. "Flutter and stall response of a helicopter blade with structural nonlinearity". *Journal of Aircraft, 29*, pp. 953–960.

[11] Tang, D. M., and Dowell, E. H., 1993. "Comparison of theory and experiment for nonlinear flutter and stall response of a helicopter blade". *Journal of Sound and Vibration, 165*, pp. 953–960.

[12] Andronov, A. A., Vitt, A. A., and Khaikin, S. E., 1966. *Theory of oscillators*. Pergamon Press LTD, New York.

[13] Kalmár-Nagy, T., Wahi, P., and Halder, A. "Dynamics of a hystereric relay oscillator with periodic forcing". *SIAM Journal on Applied Dynamical Systems*.

[14] Pratap, R., Mukherjee, S., and Moon, F. C., 1994. "Dynamic behavior of a bilinear hysteretic elastoplastic oscillator, .1. free oscillations". *Journal of Sound and Vibration, 172*, pp. 321–337.

[15] Pratap, R., Mukherjee, S., and Moon, F. C., 1994. "Dynamic behavior of a bilinear hysteretic elastoplastic oscillator .2. oscillations under periodic impulse forcing". *Journal of Sound and Vibration, 172*, pp. 339–358.

[16] Shaw, S. W., and Holmes, P. J., 1983. "A periodically forced piecewise linear-oscillator". *Journal of Sound and Vibration, 90*, pp. 129–155.

[17] Mahfouz, I. A., and Badrakhan, F., 1990. "Chaotic behavior of some piecewise-linear systems .1. systems with set-up spring or with unsymmetric elasticity". *Journal of Sound and Vibration, 143*, pp. 255–288.

[18] Mahfouz, I. A., and Badrakhan, F., 1990. "Chaotic behavior of some piecewise-linear systems, .2. systems with clearance". *Journal of Sound and Vibration, 143*, pp. 289–328.

[19] Leine, R. I., 2006. "Bifurcations of equilibria in non-smooth continuous systems". *Physica D-Nonlinear Phenomena, 223*, pp. 121–137.

[20] Sheldahl, R. E., and Klimas, P. C., 1981. Aerodynamic characteristics of seven symmetrical airfoil sections through 180-degree angle of attack for use in aerodynamic analysis of vertical axis wind turbines. Tech. rep., Sandia National Laboratories. SAND80-2114.

[21] Kriegsmann, G., 1987. "The rapid bifurcation of the wien bridge oscillator". *IEEE Transactions on Circuits and Systems,, 34*(9), sep, pp. 1093 – 1096.

[22] Freire, E., Ponce, E., and Ros, J., 1999. "Limit cycle bifurcation from center in symmetric piecewise-linear systems". *International Journal of Bifurcation and Chaos, 9*(5), pp. 895 – 907.

[23] Gantmacher, F. R., 1959. *The theory of matrices*, Vol. 2. Chelsea Publishing Company, New York.

[24] Seiranyan, A. P., 1994. "Collision of eigenvalues in linear oscillatory systems". *Journal of Applied Mathematics and Mechanics, 58*, pp. 805 – 813.

[25] Bernardo, M., Budd, C. J., Champneys, A. R., and Kowalczyk, P., 2008. *Piecewise-smooth dynamical systems : theory and applications*, Vol. 2. Springer Verlag, London.

[26] Zhusubaliyev, Z. T., and Mosekilde, E., 2003. *Bifurcations and chaos in piecewise-smooth dynamical systems*. World Scientific, River Edge, NJ.

[27] Strogatz, S. H., 2000. *Nonlinear dynamics and chaos : with applications tophysics, biology, chemistry, and engineering*. Westview Press, Cambridge, MA.

[28] Dhooge, A., Govaerts, W., and Kuznetsov, Y. A., 2003. "MATCONT: A matlab package for numerical bifurcation analysis of ODEs". *ACM Trans. Math. Softw., 29*, June, pp. 141 – 164.

[29] Elgohary, T., 2010. "Nonlinear analysis of a two dof piecewise linear aeroelastic system". Master's thesis, Texas A&M University.

[30] Hilborn, R. C., 2000. *Chaos and nonlinear dynamics : an introduction for scientists and engineers*. Oxford University Press, Oxford, NY.

[31] Jeffries, C., and Perez, J., 1982. "Observation of a pomeau-manneville intermittent route to chaos in a nonlinear oscillator". *Phys. Rev. A, 26*(4), Oct, pp. 2117–2122.

[32] Yeh, W. J., and Kao, Y. H., 1982. "Universal scaling and chaotic behavior of a josephson-junction analog". *Phys. Rev. Lett., 49*(26), Dec, pp. 1888–1891.

[33] Hayashi, H., Ishizuka, S., and Hirakawa, K., 1983. "Transition to chaos via intermittency in the onchidium pacemaker neuron". *Physics Letters A, 98*(8-9), pp. 474 – 476.